Renewable Energy 215 (2023) 118907

Contents lists available at ScienceDirect

Renewable Energy

journal homepage: www.elsevier.com/locate/renene

Guaiacol hydrotreatment in an integrated APR-HDO process: Exploring the promoting effect of platinum on Ni–Pt catalysts and assessing methanol and glycerol as hydrogen sources

Wei Jin [a,b], Jesus Gandara-Loe [c], Laura Pastor-Pérez [c,a], Juan J. Villora-Picó [d], Antonio Sepúlveda-Escribano [d], Roberto Rinaldi [e,**], Tomas Ramirez Reina [a,c,*]

[a] Department of Chemical and Process Engineering, University of Surrey, Guildford, GU2 7XH, United Kingdom
[b] School of Energy and Environment, Southeast University, 210096, Nanjing, China
[c] Department of Inorganic Chemistry and Material Science Institute, University of Seville-CSIC, 41092, Seville, Spain
[d] Laboratorio de Materiales Avanzados, Departamento de Química Inorgánica - Instituto Universitario de Materiales de Alicante, Universidad de Alicante, Apartado 99, E-03080, Alicante, Spain
[e] Department of Chemical Engineering, South Kensington Campus, Imperial College London, London, SW7 2AZ, United Kingdom

ARTICLE INFO

Keywords:
Biomass upgrading
Ni–Pt catalysts
Hydrodeoxygenation
Aqueous phase reforming

ABSTRACT

This study presents an integrated approach combining aqueous phase reforming (APR) and hydrodeoxygenation (HDO) for the hydrotreatment of guaiacol, a model compound representing lignin-derived phenols in pyrolysis bio-oils. The APR process enables in-situ H_2 generation, eliminating the need for an external hydrogen source. We examine the interplay between metal species, the Pt-promoting effect on Ni–Pt catalyst supported on activated carbon (AC), and the choice of hydrogen source (methanol or glycerol). Amongst the monometallic catalysts, a 1% Pt/AC catalyst notably achieved over 96% guaiacol conversion at 300 °C with either hydrogen source. Interestingly, when 0.5–1% of the Ni loading is replaced with Pt, the resulting bimetallic Ni–Pt/AC catalysts demonstrate a significant improvement in guaiacol conversion, reaching 70% when methanol is employed as the hydrogen source. Surprisingly, no comparable enhancement in guaiacol conversion is observed when employing glycerol as the hydrogen source. This observation underlines one of the pivotal effects of the hydrogen source on catalyst performance. X-ray photoemission spectroscopy (XPS) pinpointed strong Ni–Pt interactions in the catalyst. It also revealed distinctive electronic features of Ni–Pt/AC, which are favourable for steering selectivity towards cyclohexanol rather than phenol when Pt loading is increased from 0.5 to 1%. Moreover, Pt enhanced catalyst stability by inhibiting the oxidation of Ni sites and mitigating Ni–Pt phase sintering. Overall, our findings offer important insights into integrating APR and HDO processes, the promotion effect of Pt, and the importance of hydrogen source selection in terms of guaiacol conversion and catalyst stability.

1. Introduction

The increasing depletion of petroleum reserves and rising demand for environmentally sustainable energy sources have driven research efforts towards advanced synthetic biofuels [1,2]. These biofuels offer potential drop-in replacements for fossil fuels in sectors such as aviation, shipping, and heavy freight lorries, where electrification remains a significant challenge. To meet the long-term climate targets outlined in the Paris Agreement [1,2] and the 2030 UN Sustainability Goals [3], it is crucial to pursue sustainable production of advanced biofuels through the utilisation of lignocellulosic biomass waste [4]. In this context, pyrolysis of lignocellulosic biomass waste yields a pyrolysis oil or bio-oil that offers an entry point towards sustainable production of energy-dense biofuels [5–10]. However, bio-oils feature a high content of oxygenated compounds (45–50%) and water (15–35%). This poses significant challenges for direct use or blending as fuel feedstock [5–10].

Employing zeolite-catalysed cracking or hydrodeoxygenation (HDO) to reduce the oxygen content of bio-oil has extensively been studied

* Corresponding author. Department of Inorganic Chemistry and Material Science Institute, University of Seville-CSIC, 41092, Seville, Spain.
** Corresponding author.
E-mail addresses: r.rinaldi1@imperial.ac.uk (R. Rinaldi), tramirez@us.es (T.R. Reina).

https://doi.org/10.1016/j.renene.2023.118907
Received 19 February 2023; Received in revised form 26 May 2023; Accepted 9 June 2023
Available online 10 June 2023

[11–15]. Zeolite-catalysed cracking processes often face issues with fast catalyst deactivation due to coke formation. In stark contrast, HDO of bio-oils shows better catalyst durability [16–19]. Current research has shown that complete HDO of pyrolysis oil is not always necessary for fuel applications, as the effects of oxygenates on fuel quality vary depending on their type and oxygenated group position [11]. Cyclohexanol additives in petrol-ethanol and diesel blends have demonstrated improved combustion properties and reduced emissions [12,13], emphasising the potential of these blends as cleaner, more efficient fuel options in the pursuit of sustainable energy solutions [14,15]. Despite its potential, HDO remains a hydrogen-intensive process, with current industrial hydrogen production heavily dependent on fossil carbonaceous feedstocks and, thus, associated with significant CO_2 emissions [16,17]. Therefore, an essential step towards mitigating CO_2 emissions in the sustainable production of energy-dense biofuels is the development of HDO processes that are self-sufficient in H_2 [18,19].

Integrating aqueous-phase reforming (APR) and hydrodeoxygenation (HDO) has the potential for practical applications in the transformation of bio-derived compounds into energy-dense molecules, utilising alcohols and polyols as sources of hydrogen [20]. Owing to their shared optimal reaction conditions and similar catalyst compatibility, hydrogen produced in the APR of alcohols and polyols can be readily consumed in the HDO process to treat oxygenated compounds in bio-oils. In this instance, Lemonidou et al. demonstrated the selective hydrogenolysis of glycerol with in-situ supplied hydrogen via APR, using methanol or ethanol as the hydrogen source [47]. Under optimised conditions, nearly complete conversion of glycerol (95.9%) was achieved, with a high selectivity (79.4%) to 1,2-propanediol at 250 °C using a Cu catalyst, provided the methanol-to-glycerol ratio was maintained at 4:1 (v/v) [47].

The selectivity of hydrogen production from the APR of biomass-derived compounds using Pt-based catalysts is generally observed to follow the sequence: methanol > ethylene glycol > glycerol > sorbitol > glucose [39,40]. Methanol, which can be produced from renewable resources such as biomass-derived polyols, sugars [41], glycerol, or through the demethoxylation of lignin [42], has been studied as an effective hydrogen source in combined APR-HDO processes [43,44], as indicated by chemical equation (1). Glycerol, a low-cost and readily available by-product of the biodiesel industry, also presents potential as a hydrogen source, as shown by chemical equation (2) [46]:

$$\text{Methanol APR: } CH_3OH + H_2O \rightleftharpoons 3H_2 + CO_2 \quad (1)$$

$$\text{Glycerol APR: } C_3H_8O_3 + 2H_2O \rightarrow 7H_2 + 3CO_2 \quad (2)$$

Recent research has focused on the HDO of bio-oils [33–35] and lignin model compounds, such as guaiacol [36–38], using H_2 pressures in the hydrotreatment process. However, integrating APR and HDO into a one-pot tandem process has garnered far less attention. One notable example demonstrated a full conversion of guaiacol to cyclohexane with a high selectivity of 93.4%, utilising a Ni-based catalyst in an HDO process sustained by H_2 derived from the APR of methanol [45]. This finding demonstrated a concept of upgrading oxygenated bio-compounds derived from lignin with no external H_2 supply.

Ni and Pt-based catalysts show promise for integrated APR-HDO processes due to their high activity in reforming and hydrogenolysis processes [21,22]. Bimetallic catalysts exhibit modified electronic and geometric structures on their metal surfaces, distinguishing them from monometallic counterparts. These unique characteristics enable bimetallic catalysts to possess tunable chemical and physical properties, enhancing selectivity towards desired products. [23,24]. Moreover, incorporating Ni as a component of noble bimetallic catalysts a cost-effective approach to reducing noble metal content in catalyst compositions [25]. Notably, bimetallic Ni–Pt catalysts have proven effective in deoxygenating fatty acids [26–28]. Previous research conducted by our team demonstrated that activated carbon (AC) is highly suitable as a support for metal catalysts in deoxygenating pyrolysis bio-oils and model compounds with or without the input of external H_2 [48]. This is attributed to the hydrophobicity and exceptional textural properties of activated carbons [49,50].

Despite these preliminary achievements, there is still limited information in the literature regarding the intricate relationship between metal species in Ni–Pt/AC catalyst and the impact of the choice of hydrogen source (methanol or glycerol) on guaiacol conversion and product distribution in addition to catalyst stability in recycling experiments.

This study investigates the fundamental aspects of designing Ni–Pt/AC catalysts for upgrading lignin-derived phenolics into energy-dense synthetic biofuels. Lignin, formed in plants through the polymerisation of functionalised C_9 phenylpropane units (*p*-coumaryl alcohol, coniferyl alcohol, and sinapyl alcohol), is a valuable resource for producing energy-dense transportation fuels. This is owing to the higher C-atom counts of lignin products formed in the pyrolysis of waste plant biomass than those derived from cellulose and hemicellulose [29–32]. Within this context, we chose guaiacol as a representative model compound of lignin-derived products in pyrolysis bio-oils. Herein, we examine the impact of substituting the Ni loading in a 15% Ni/AC catalyst with small amounts of Pt (0.5–1%) on the catalyst performance of the resulting bimetallic Ni–Pt/AC catalysts in the guaiacol hydrotreatment via an integrated APR-HDO process. To optimise the guaiacol conversion in the integrated APR-HDO process, we explore the impact of various process parameters, including the choice of metal species (Pt and Ni), the Pt loading, and the type of hydrogen source (methanol or glycerol). Additionally, we conduct a detailed assessment of the recyclability of the most effective catalysts, demonstrating the impact of the hydrogen source on the catalyst recyclability.

In this study, our overarching objective is to contribute fundamental chemical insights that can underpin the technical development of tandem APR-HDO reactions to upgrade lignin-derived phenolics. By doing so, the requirement for external H_2 supply can be eliminated, thereby enhancing the environmental sustainability of these processes in the context of using bio-oils as raw material for producing advanced biofuels.

2. Materials and methods

2.1. Materials

The chemicals used to synthesise the catalysts, including nickel nitrate hexahydrate and chloroplatinic acid hexahydrate, were supplied by Sigma Aldrich. Activated carbon (RGC 30) was provided by Westvaco. Guaiacol, solvents (ethyl acetate and acetone), hydrogen source (methanol or glycerol), and chemicals used for calibration (including cyclohexanol, cyclohexanone, anisole, phenol, *o*-cresol, and catechol) were also supplied by Sigma Aldrich.

2.2. Synthesis of catalysts

Ni-based monometallic catalyst, labelled as 15Ni/AC, was prepared via wet impregnation to obtain a catalyst with 15 wt% Ni loading. Nickel nitrate hexahydrate was dissolved in the necessary acetone to wet the activated carbon. Prior to the synthesis, the activated carbon (AC) was dried in the oven, added to the Ni solution, and stirred for 4 h. The solvent was slowly removed under reduced pressure at 60 °C. Finally, the solid was dry at 80 °C for 24 h and treated for 4 h at 350 °C under flowing N_2. Using a similar procedure, the Pt-based monometallic catalyst, labelled 1Pt/AC, was synthesised using chloroplatinic acid as the precursor and water as the solvent to obtain a catalyst with a 1 wt% Pt loading. Bimetallic Ni–Pt carbon-supported catalysts, with different Ni:Pt ratios, 14.5%Ni-0.5%Pt and 14%Ni–1%Pt, were further synthesised via co-impregnation. These bimetallic catalysts were labelled as 14.5Ni0.5Pt/AC and 14Ni1Pt/AC. Before the activity tests, all synthesised catalysts were pre-reduced for 2 h at 350 °C under a gas flow of

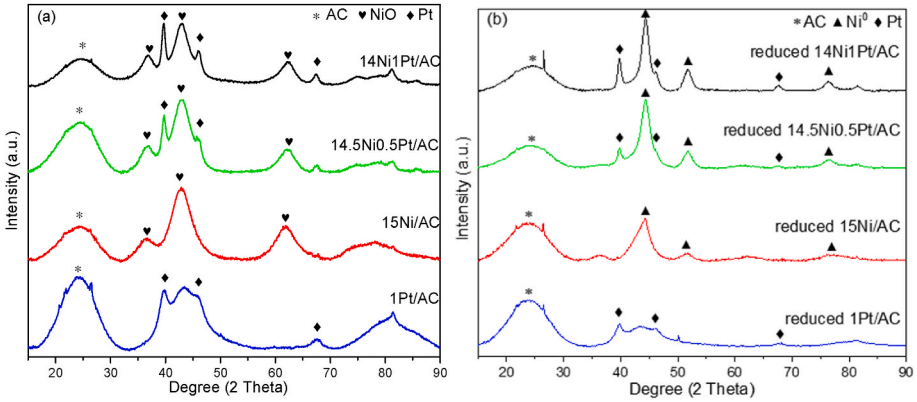

Fig. 1. XRD analysis of Ni-based catalyst precursors and reduced catalysts. (a) XRD patterns for catalyst precursors treated under N_2 atmosphere, with reflections characteristic for NiO face-centred cubic phase. (b) XRD patterns for catalysts reduced under an H_2 atmosphere, showing the presence of the metallic Ni phase indicating the reduction of the NiO phase. Both (a) and (b) present a broad background signal characteristic for carbon supports (shown by '*' and the characteristic reflections for Pt, with the latter suggesting a "pre-reduction" of PtO_x in the thermal treatment under the N_2 atmosphere.

100 mL/min (H_2:N_2 = 1:4).

2.3. Characterisation methods

2.3.1. X-ray diffraction measurements (XRD)

XRD diffraction patterns were recorded on a Bruker D8-Advance with a Göebel mirror and a Kristalloflex K 760-80 F X-Ray generation system fitted with a Cu cathode and a Ni filter. Spectra were registered between 10 and 80° (2θ) with a step of 0.05° and a time per step of 3s.

2.3.2. Transmission electron microscopy (TEM)

TEM analysis was conducted with a JOEL model JEM-210 electron microscope working at 200 kV and equipped with an INCA Energy TEM 100 analytical system and an SIS MegaView II camera. Samples for analysis were suspended in methanol and placed on copper grids with holey-carbon film support.

2.3.3. Hydrogen temperature-programmed reduction H_2-TPR

H_2-TPR measurements were conducted on the calcined catalysts in a U-shaped quartz reactor using a 5% H_2/He gas flow of 50 mL/min, with a heating rate of 10 °C/min. Samples were treated under a He flow at 150 °C for 1 h before the measurement to remove adsorbed molecules. The hydrogen consumption was followed by online mass spectrometry (Pfeiffer, OmniSter GSD 301).

2.3.4. X-ray photoelectron spectroscopy (XPS)

XPS measurements were performed with a K-ALPHA spectrometer (ThermoFisher Scientific) operated in the constant energy mode with survey scan pass energies of 200 eV and narrow scan energies of 50 eV to measure the whole energy band as well as selectively measure particular elements. All XP spectra were acquired using Al-Kα radiation (1486.6 eV), operating at 3 mA and 12 kV with a twin crystal monochromator, yielding an elliptical focused X-ray spot (with a primary axis length of 400 μm). Charge compensation was attained with the system flood gun, which provides low energy electrons and argon ions from a single source. The C1*s* core level was used for the reference binding energy (284.6 eV). All samples were reduced *ex-situ* and kept in octane. Before recording the spectrum, the samples were placed in the analysis chamber until a residual pressure of ca. 5×10^{-7} N/m^2 was reached.

2.4. Catalytic activity test

The integrated APR-HDO experiments were conducted in a high-pressure batch reactor using PTFE gaskets (Parr Series 5500 HPCL Reactor with a 4848 Reactor Controller). In a 250 mL glass-lined steel vessel, guaiacol (0.5 g), hydrogen source (methanol or glycerol, 0.5 g) in water (total mass: 50 g), and catalyst (0.2 g) were loaded. To avoid air contamination, the reaction solution was deaerated by passing an N_2 flow under a stirring speed of 300 rpm for 5 min before closing the reaction vessel. Then, the reactor was heated to the desired temperature (300 °C) and held at this temperature of 4 h under a stirring speed of 300 rpm. The autogenous pressure was 100 bar during the reaction. After the reaction, the spent catalyst was recovered from the liquid by filtration followed by drying treatment. The organic products were dissolved and recovered with ethyl acetate extraction. Reproducibility was analysed, and the result deviation was ±2%.

The organic products were identified by gas chromatograph-mass spectrometry (GC-MS). Quantitative analysis was performed with a gas chromatograph-flame ionisation detector (GC, Shimadzu; FID: Agilent cellular model). In both analyses, the injector temperature was kept at 280 °C. GC separation was performed by using a Carboxen Packed Analytical Column (30 m × 320 μm × 0.25 μm). A split ratio of 8:1 was held. The column was firstly held at 50 °C for 1 min, then increased to 240 °C at a heating rate of 5 °C/min and held at 240 °C for 10 min. Guaiacol and typical products were quantified based on the external standard method.

Conversion of guaiacol and the selectivity towards typical products (based on C mol) were calculated using equations (3) and (4) [51]:

$$\text{Conversion of guaiacol} = \frac{n_{GUA,in} - n_{GUA,out}}{n_{GUA,in}} \times 100\% \quad (3)$$

$$\text{Selectivity to product } x = \frac{n_x \times N_x}{\left(n_{G,in} - n_{G,out}\right) \times N_{GUA}} \times 100\% \quad (4)$$

where, *GUA:* guaiacol; $n_{GUA,in}$ = Initial amount of guaiacol (in mol); $n_{GUA,out}$ = Detected amount of guaiacol in the organic phase (in mol); n_x = amount of a product *x* (in mol). N_{GUA} = carbon atom count in guaiacol (7); N_x = carbon atom count in the product *x*.

3. Results and discussion

3.1. Catalysts characterisation

3.1.1. X-ray diffraction measurements (XRD)

To characterise the structural features of the synthesised materials, XRD analyses for both N_2-treated and reduced materials were performed in the 2θ range from 10° to 90°. XRD patterns are shown in Fig. 1a and b for the catalyst precursors (treated under N_2 atmosphere) and reduced catalysts (reduced under H_2 atmosphere). All XRD patterns present a broad background signal at *ca.* 24.5° (amorphous halo characteristic for carbon supports) [52]. In Fig. 1a, for Ni-based catalyst precursors (Ni/AC, 14.5Ni0.5Pt/AC and 14Ni1Pt/AC), the reflections characteristic for NiO face-centred cubic phase at 37.2° (111), 43.3° (200), and 62.9° (220) were detected [53]. As for the XRD patterns of the reduced catalysts (Fig. 1b), the reflections at around 44.5° (111), 51.8° (200) and 76.4° (220) confirm the presence of the metallic Ni phase, demonstrating the reduction of the NiO phase [54,55]. Notably, the reflections characteristic of PtO_x species were not observed in the XRD patterns of

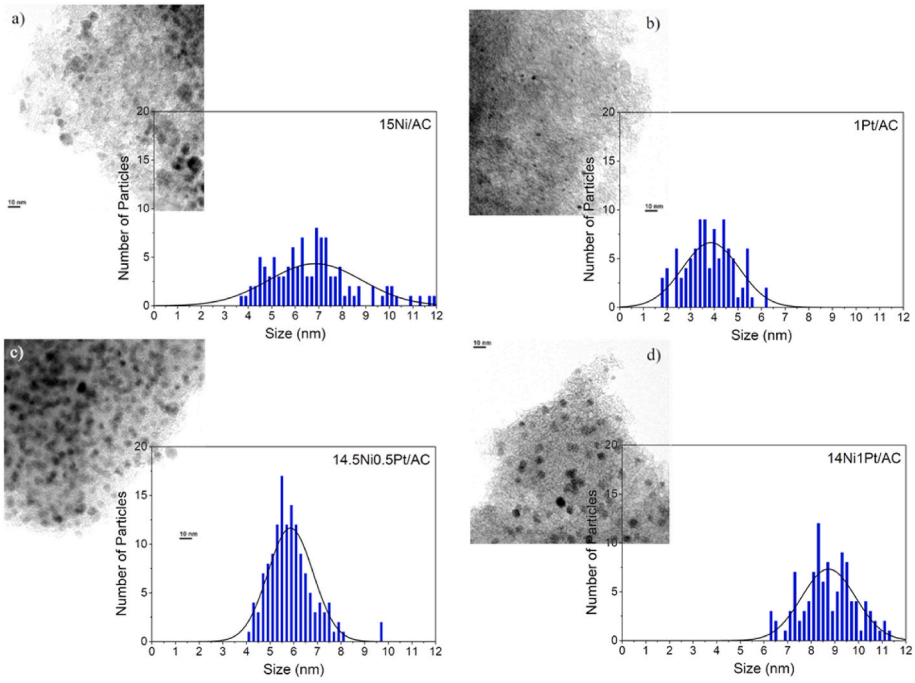

Fig. 2. TEM images and particle size histograms for reduced catalysts. (a) Presents a broad size distribution of Ni nanoparticles averaging 7 nm. (b) Displays a uniform distribution of Pt nanoparticles averaging 3.5 nm in size. (c) and (d) Show the Ni–Pt/AC catalysts with uniformly dispersed bimetallic nanoparticles on the carbon support. For 14.5Ni0.5Pt/AC and 14Ni1Pt/AC, the average size of Ni–Pt nanoparticles is 5.8 nm and 9 nm, respectively.

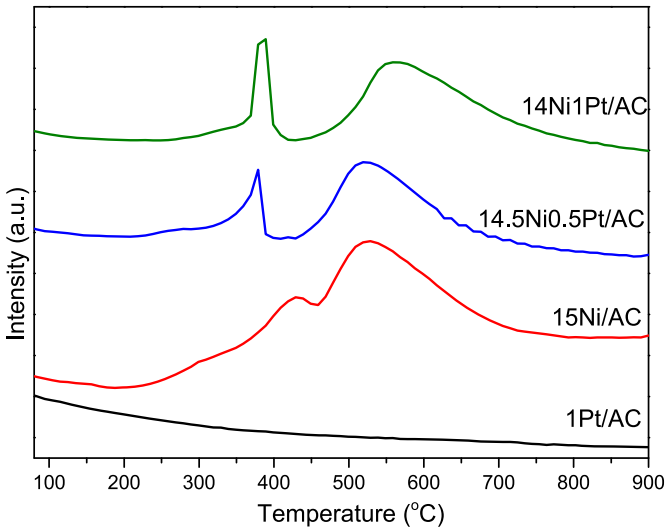

Fig. 3. H_2-TPR profiles of catalyst precursors, indicating metal-metal and metal-support interactions and their redox properties. The results corroborate a synergistic effect of Pt on NiO_x redox properties affecting the formation of Ni nanoparticles and hinting at a potential hydrogen spillover from Pt sites to NiO species in bimetallic systems.

the bimetallic catalyst precursors treated under an N_2 atmosphere. Instead, the peaks at 39.6, 47.4 and 67.1°, corresponding to the metallic Pt reflections (111), (200), and (220), respectively, were found for both catalyst precursors and reduced catalysts. In line with previous reports, a pre-reduction of PtO_x took place in the thermal treatment under the N_2 atmosphere; such a process can utilise the activated carbon as a source of reducing species [56]. Moreover, in terms of Pt dispersion, no apparent difference was observed between the reflections of Pt (or PtO_x) in XRD patterns for Ni–Pt/AC and Pt/AC catalysts. Therefore, Ni does not favour the further dispersion of Pt in the Ni–Pt/AC catalysts.

3.1.2. *Transmission electron microscopy (TEM)*

To gain further insights into the features of Ni, Pt and Ni–Pt nanoparticles in the reduced catalysts, the materials were analysed by TEM. Fig. 2 shows TEM images and particle size distribution histograms of the reduced catalysts from which information related to the metal nanoparticle size and active phase distribution can be extracted. Fig. 2a presents a uniform dispersion of Ni particle size of *ca.* 7 nm showing a broad size Ni cluster distribution between 4 and 12 nm. The distribution of Pt nanoparticles is observed in Fig. 2b, indicating particles with an average size of 3.5 nm. Fig. 2c and d display the TEM images of the Ni–Pt/AC catalysts and confirm uniform nanoparticle dispersions on the AC support with no large particle cluster agglomeration. Furthermore, the Ni–Pt nanoparticles feature narrow particle size distribution. For 14.5Ni0.5Pt/AC and 14Ni1Pt/AC, the average size of Ni–Pt nanoparticles is 5.8 nm and 9 nm, respectively. This confirms the positive role of Pt in the dispersion of the bimetallic active phase [57]. The presence of 0.5–1.0% of Pt in the bimetallic catalyst formulation also makes Ni–Pt nanoparticles more resistant to sintering in the integrated APR-HDO process (*vide infra*).

3.1.3. *Hydrogen temperature-programmed reduction (H_2-TPR)*

A comprehensive analysis was conducted on the redox properties of the catalysts and the interactions that occurred between the metals and supports, based on the data obtained from H_2-TPR measurements. H_2-TPR profiles of the catalyst precursors are shown in Fig. 3.

Notably, in the TPR profile of 1Pt/AC catalyst precursor, no H_2 consumption peak was observed. Typically, the reduction of PtO_x over AC generates an H_2 consumption peak at around 180 °C [58]. As demonstrated by the XRD results (Fig. 1a), the reduction of PtO_x had already occurred during the catalyst precursor synthesis in the thermal treatment stage under N_2 atmosphere (*i.e.*, before the H_2-TPR experiment). Under these conditions, the H_2-equivalent needed for the Pt reduction can be obtained from the partial decomposition of the carbon support [56]. In the TPR profile of 15Ni/AC precursor, three broad reduction zones centred at 350 °C, 445 °C, and 545 °C are observed. The first can be attributed to the reduction of a small amount of bulk NiO

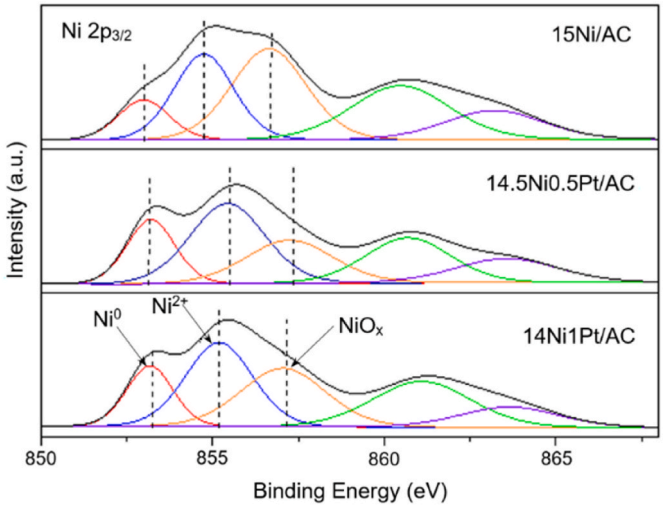

Fig. 4. XP spectra of the Ni 2*p* core levels, providing insights into the changes in the electronic structure of the active species after the reduction treatment.

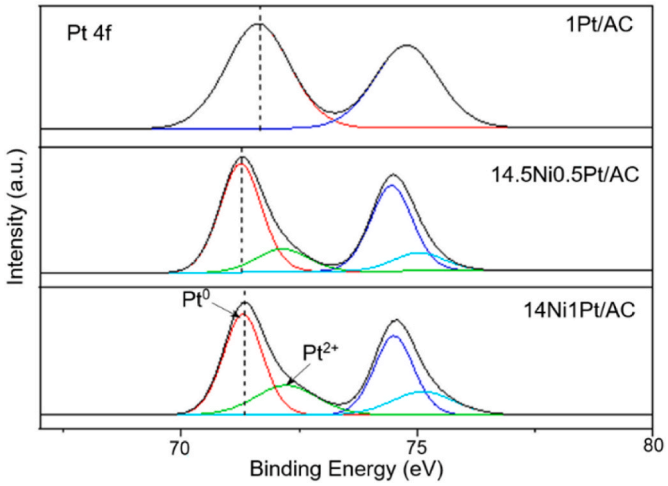

Fig. 5. XP spectra of the Pt 4*f* core levels, shedding light on the alterations in the electronic structure post-reduction.

[59] followed by the reduction of a wide variety of NiO_x species between 445 °C and 545 °C [60,61]. This observation appears to be associated with generation of a non-uniform Ni size particle distribution by reduction processes on 15Ni/AC precursor, as revealed by TEM imaging (Fig. 2a).

In contrast, for the bimetallic Ni–Pt/AC catalyst precursors, one narrow and another broad reduction zones of H_2 consumption were identified in the H_2-TPR profiles. These reduction zones presented a temperature lower than that found for the 15Ni/AC catalyst. As seen in the TEM images for 14.5Ni0.5Pt/AC and 15Ni1Pt/AC reduced catalysts (Fig. 2c and d, respectively), Pt plays a crucial role in controlling the uniformity of Ni particle size distribution. Putting these pieces of information together, the results corroborate a synergistic effect of Pt on NiO_x redox properties which impacts the formation of uniform Ni–Pt nanoparticles, which are well dispersed on the AC support for both 14.5Ni0.5Pt/AC and 15Ni1Pt/AC catalysts. Previous reports have associated such an outcome with a synergistic effect with the hydrogen spillover from Pt sites to NiO species, thus decreasing NiO reduction temperature on bimetallic systems [61,62].

3.1.4. *X-ray photoelectron spectroscopy (XPS)*

To evaluate the changes in the electronic structure of the active species after reduction treatment, the X-ray photoemission (XP) spectra of the reduced catalysts were collected. Figs. 4 and 5 present the XP spectra of Ni 2*p* and Pt 4*f* core levels, respectively. The binding energy values (BE) for the deconvoluted peaks of Ni $2p_{3/2}$ and Pt $4f_{7/2}$, the different metal/oxide and metal/support ratios estimated from the XP spectra are summarised in Table 1.

Table 1
Binding energy values (BE) of Ni $2p_{3/2}$ and Pt $4f_{7/2}$ core levels and metal/oxide and metal/support ratios.

Catalysts	Ni $2p_{3/2}$				Pt $4f_{7/2}$		
	Ni^0	Ni^{2+}	Ni^0/Ni^{2+}	Ni^0/AC	Pt^0	Pt^{2+}	Pt^0/Pt^{2+}
	B.E. (eV)	B.E. (eV)	at./at.	At./at.	B.E. (eV)	B.E. (eV)	at./at.
15Ni/AC	853.0	854.7	0.17	0.16	–	–	–
1Pt/AC	–	–	–	–	71.6	–	–
14.5N0.5Pt/AC	853.2	855.4	0.32	0.22	71.3	72.1	3
14Ni1Pt/AC	853.2	855.2	0.27	0.22	71.3	72.2	2

XP spectra of the Ni $2p_{3/2}$ were deconvoluted in three prominent peaks (Fig. 4), proposed for three main types of nickel species co-existing on the catalyst surface. The first peak (853 eV) is assigned to Ni^0 species. The second peak (855 eV) is assigned to Ni^{2+} species [63,64]. Finally, the third peak (857 eV) is proposed for Ni^{2+} vacancies in the NiO crystal lattice [65,66]. Defective NiO structures are suitable for the targeted activation of C–O bonds. In this manner, such surface defects can serve as active sites for activating organic molecules towards HDO processes.

Moreover, substituting a part of the Ni loading with Pt slightly shifts the BE values of Ni^{2+} species to a higher value in the resulting Ni–Pt/AC catalysts. This observation demonstrates the Ni–Pt interaction. Furthermore, the Ni–Pt/AC catalysts exhibit Ni^0/Ni^{2+} ratios higher than that found for Ni/AC. This piece of evidence indicates that the presence of Pt in the Ni–Pt/AC catalysts facilitates the stabilisation of Ni species in the reduced state. This observation agrees with the TPR results (Fig. 3), corroborating the general claim that the addition of noble metals enhances the reducibility of Ni particles [67].

As shown in Figure 5, 1Pt/AC catalyst presents only one contribution to the XP spectra on Pt $4f_{7/2}$ and $4f_{5/2}$ states, confirming the presence of Pt^0 only. Focusing on the $4f_{7/2}$, a shift to lower BE values in the Ni–Pt/AC catalysts is observed, confirming the electronic environment modification due to the interaction with Ni in the Ni–Pt/AC catalysts [68]. Notably, the Ni–Pt interaction XP signal creates an additional XP signal (at 72.1–72.2 eV) corresponding to Pt^{2+}. This signal appears to be associated with the promoting effect of Pt on Ni reduction, as revealed by the increase in Ni^0/Ni^{2+} ratios found for Ni–Pt/AC catalysts. Overall, Pt favours Ni reduction due to close metal-metal interaction and electronic transfer from Pt to Ni. This observation confirms our working hypothesis that electronically rich Ni species at the Pt–Ni interface, in addition to defective NiO_x species, coexist in Ni–Pt/AC catalysts. The proposed features are involved in the performance of Ni–Pt/AC catalysts in the guaiacol hydrotreatment via the integrated APR-HDO process (*vide infra*).

3.2. *HDO of guaiacol*

Fig. 6 presents the reaction network in converting guaiacol into cyclohexanol in the integrated APR-HDO process to guide the readers through the discussion in the next sections.

The conversion of guaiacol into cyclohexanol is proposed to involve four aromatic intermediates in the specific order of importance: catechol > phenol ≫ anisole. In the integrated APR-HDO process, the hydrogenation of phenol to cyclohexanone and cyclohexanol constitutes H_2-intensive processes. Logically, the increased share of these compounds in the product distributions serves as an indicator of improved

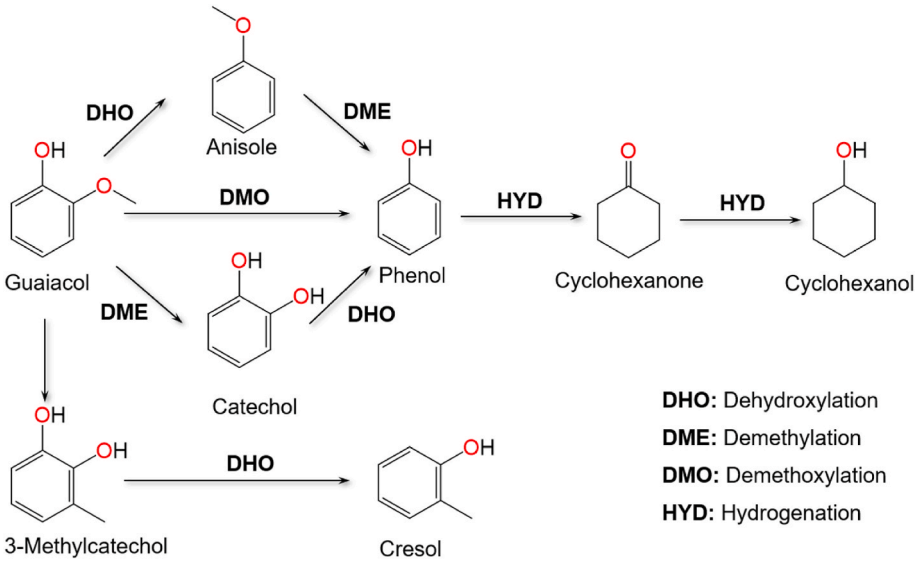

Fig. 6. The reaction network proposed for the conversion of guaiacol into cyclohexanol in the integrated APR-HDO process.

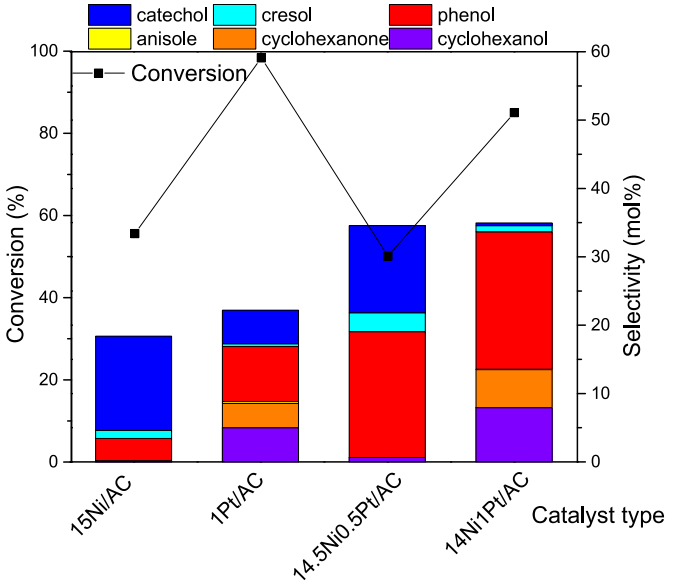

Fig. 7. Results of guaiacol conversion in the integrated APR-HDO process using methanol as the hydrogen source. Reaction conditions: guaiacol (0.5 g), methanol (0.5 g) dissolved in water (total mass of 50 g), and catalyst (0.2 g) were processed in a batch reactor (200 mL), operating at 300 °C, 4 h, under an autogenous pressure of 100 bar. The reactor was equipped with an overhead stirrer set at 300 rpm.

catalyst's ability to activate methanol or glycerol in the APR process, generating sufficient H_2 for the hydrogenation of phenol. The formation of 3-methylcatechol, although not detected in the product mixtures, is suggested as a possible route for cresol formation. Cresol is proposed to be an endpoint in the reaction network. This is because eventual demethylation via thermal cracking of the Csp^2—Csp^3 bonds is less likely under the reaction conditions of this study. Moreover, Ni catalysts present poor activity towards the hydrogenolysis of Csp^2—Csp^3 bonds [80,81].

The results and discussion in this section are divided into two parts. The first part focuses on the findings from the APR-HDO processes utilising methanol as the hydrogen source, while the second part compares the use of glycerol as the hydrogen source.

3.3. Methanol as the hydrogen source

To examine the performance of the synthesised catalysts in the guaiacol conversion in the integrated APR-HDO process using methanol as the hydrogen source, a solution containing 1 wt% guaiacol and 1 wt% methanol in water was subjected to each catalyst in a batch process at 300 °C for 4 h. Fig. 7 compares the results obtained from these experiments.

In Fig. 7, the guaiacol conversion ranges from 54% to 98% in the integrated APR-HDO process using methanol as the hydrogen source. As expected, 1Pt/AC emerges as the most active catalyst, achieving a remarkable 98% guaiacol conversion. In sharp contrast, 15Ni/AC is the least active catalyst, resulting in only a 54% guaiacol conversion. These findings are consistent with prior research, which reported higher catalytic activity for Pt than Ni in both the APR of methanol [71,72] and HDO of guaiacol [73]. Notably, the bimetallic Ni–Pt/AC catalysts exhibit a decrease in guaiacol conversion compared to the monometallic Pt catalyst. Nevertheless, the conversion levels (85% for 14Ni1Pt/AC) remain significantly higher than that obtained with 15Ni/AC (55%). This phenomenon seems related to electronic interactions between Ni and Pt, favouring Ni dispersion and enhancing redox properties. However, the presence of Ni in the bimetallic catalysts does not improve Pt particle size or the Pt^0/Pt^{2+} ratio—both of which are critical factors in the APR of methanol [74]. This is evidenced by the XRD patterns of the bimetallic catalysts (Fig. 1) and the Pt^{2+} peak in the XP spectra (Fig. 5).

It is also clear from Fig. 6 that 15Ni/AC catalyst presents a preferential selectivity to aromatic products (catechol, phenol, cresol), suggesting a limited catalytic activity for hydrogenation while using methanol as a hydrogen source. This may be associated with the inhibitory effect of methanol on the activity Ni catalysts in the hydrogenation of phenolic compounds under an H_2 pressure or via H-transfer reactions [69,70,75]. In stark contrast, 1Pt/AC catalyst shows high selectivity to hydrogenated products (cyclohexanol and cyclohexanone) and phenol. Finally, anisole was produced at very low levels in the HDO of guaiacol over 1Pt/AC catalyst. Overall, these results contrast with those by Pastor-Perez et al. reporting the guaiacol HDO reaction under H_2-free conditions reaching considerable values of conversion (*ca.* 40–60%) and selectivity to catechol under mild conditions using a Pt-based catalyst to generate H_2 through water activation [50].

Notably, the formation of saturated compounds in the presence of 1Pt/AC indicates that more H_2 is available for the HDO process. This observation corroborates the unique properties of 1Pt/AC catalyst in promoting the APR of methanol, generating the amount of H_2 required

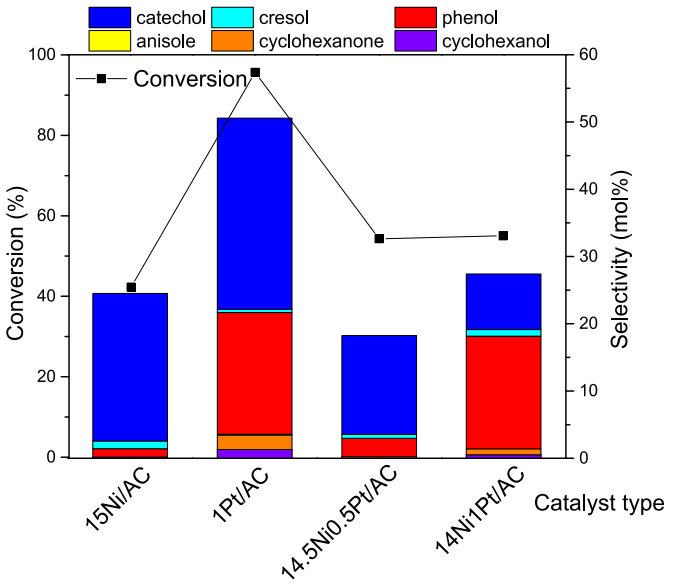

Fig. 8. Results of guaiacol conversion in the integrated APR-HDO process using glycerol as the hydrogen source. Reaction conditions: guaiacol (0.5 g), glycerol (0.5 g) dissolved in water (total mass of 50 g), and catalyst (0.2 g) were processed in a batch reactor (200 mL), operating at 300 °C, 4 h, under an autogenous pressure of 100 bar. The reactor was equipped with an overhead stirrer set at 300 rpm.

for the hydrogenation of phenol to cyclohexanol and cyclohexanone [76,77]. Moreover, compared to Ni catalysts, Pt catalysts are often less sensitive to the inhibitory effects of methanol on the saturation of phenolic compounds [78].

Compared to the 15Ni/AC catalyst, the guaiacol conversion via the integrated APR-HDO process, using the 14.5Ni0.5Pt/AC and 14Ni1Pt/AC bimetallic catalysts, exhibited enhanced selectivity towards partially deoxygenated aromatic compounds, such as cresol and phenol, as well as saturated oxygenates, including cyclohexanone and cyclohexanol. Notably, a rise in the Pt content from 0.5 to 1% in the Ni–Pt/AC catalyst led to a reduction in the presence of catechol in the product distribution of the reaction mixture.

As highlighted in the characterisation section, the strong interaction between Ni and Pt generates NiO_x vacancies. These vacancies act as efficient sites for activating the C–O bonds in guaiacol and catechol, thereby promoting guaiacol DME and catechol DHO. Additionally, the increased Ni^0/Ni^{2+} ratio, due to the addition of Pt to the catalyst composition, seems to be linked with the increased formation of cyclohexanol and cyclohexanone when the 14Ni1Pt/AC catalyst is employed. This can be ascribed to the improved generation of H_2 via APR of methanol, along with a Ni–Pt synergy favouring DMO, DME, and hydrogenation reactions. As a result, a larger proportion of saturated oxygenates in the product mixture is observed in Fig. 4, compared to the product mixture obtained from the experiment with the 15Ni/AC catalyst.

3.4. Glycerol as the hydrogen source

Competitive adsorption was recently identified in the HDO of guaiacol by catalytic hydrogen-transfer reactions using organic molecules as hydrogen sources [79,80]. In this context, glycerol presents great affinity towards Ni surfaces in catalytic transfer hydrogenation [79,80]. Furthermore, it has been reported that glycerol forms a bidentate interaction with the Ni surface, resulting in more significant competitive adsorption than methanol [83]. Hence, the effects of competitive adsorption of hydrogen source and substrate are expected to be more pronounced with glycerol than with methanol upon the

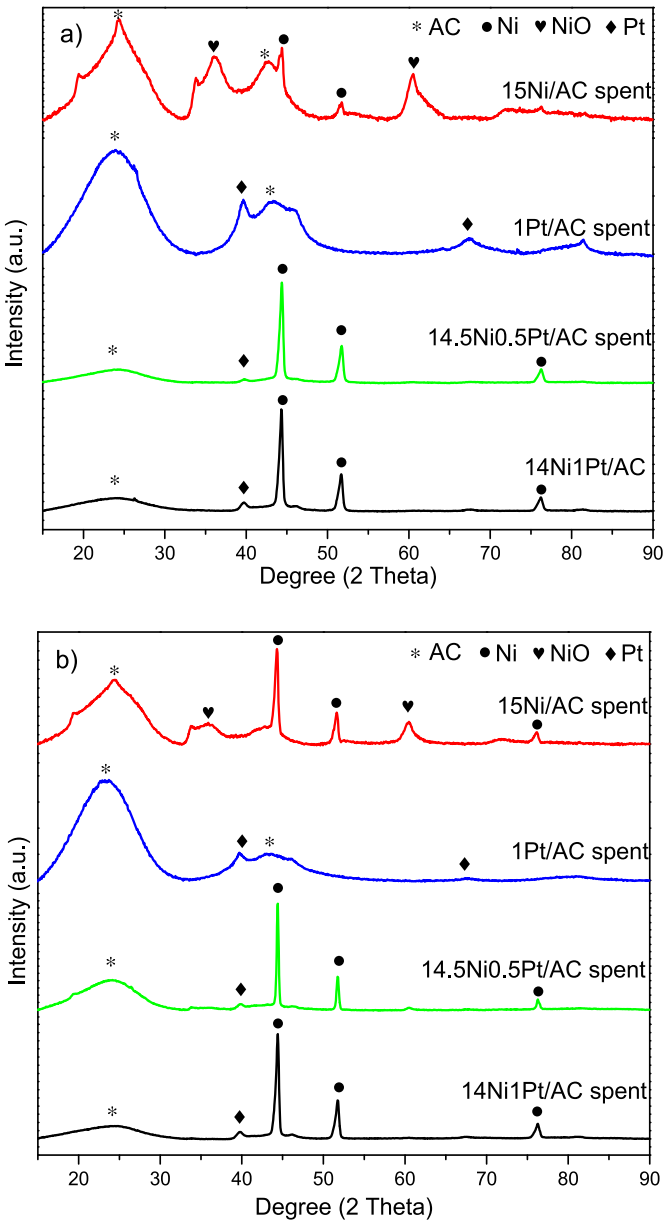

Fig. 9. XRD patterns of spent catalysts in the guaiacol conversion in the integrated APR-HDO using (a) methanol or (b) glycerol as the hydrogen source.

catalytic upgrading of guaiacol. To examine the impact of glycerol in the integrated APR-HDO process, the synthesised catalysts were tested in the guaiacol conversion using glycerol as the hydrogen source (Fig. 8).

Amongst the catalysts, 1Pt/AC catalyst achieved the highest guaiacol conversion at 96%, almost matching the 98% conversion observed when methanol was used as the hydrogen source. In turn, the bimetallic catalysts demonstrated moderate guaiacol conversion (54% for 14.5Ni0.5Pt/AC and 55% for 14Ni1Pt/AC), albeit still surpassing the results obtained with 15Ni/AC (42%). Interestingly, employing glycerol as the hydrogen source largely suppresses aromatics saturation. The guaiacol hydrotreatment led to catechol and phenol as the main products regardless of the catalyst employed.

By comparing the data from Figs. 7 and 8, the increased conversion of guaiacol when Pt is incorporated into the catalyst compositions is tied to an improved APR of methanol and, to a lesser extent, glycerol. For the latter, there exists an additional complicator. The glycerol APR is sensitive to particle size and metal distribution. Wawrzetz et al. demonstrated that augmenting the Pt particle sizes resulted in a reduction in

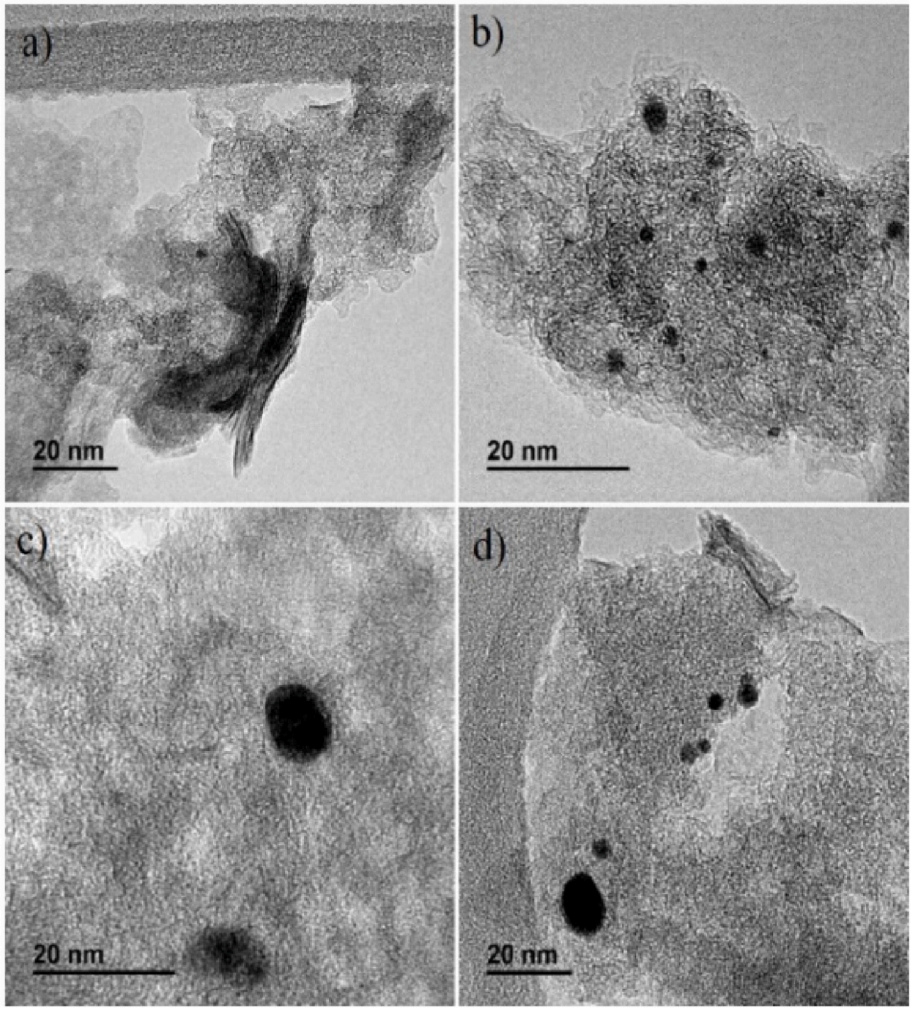

Fig. 10. TEM images of spent catalysts utilised in guaiacol conversion in the integrated APR-HDO process using methanol as the hydrogen source: a) 15Ni/AC, b) 1Pt/AC, c) 14.5Ni0.5Pt/AC and d) 14Ni1Pt/AC.

the production of H_2 and CO_2 [73]. This observation translated into less H_2 available for the reductive processes involved in the guaiacol conversion. As a result, the saturation of aromatic intermediates is hindered. Moreover, although Pt plays a beneficial role in enhancing Ni dispersion and electronic properties in the Ni–Pt/AC catalysts, the resulting enlargement in Ni–Pt nanoparticle sizes and the creation of Pt^{2+} sites appear to be detrimental to the overall performance of the APR-HDO process when using glycerol as the hydrogen source.

3.5. Post-reaction catalyst characterisation

Following the catalytic tests, the catalysts underwent characterisation using X-ray diffraction (XRD) and transmission electron microscopy (TEM). These analyses evaluated the potential impact of coking and sintering on the catalysts, as these processes typically involve catalyst deactivation mechanisms.

3.5.1. X-ray diffraction patterns (XRD)

Presented in Fig. 9a and b are the XRD pattern of the spent catalysts employed in the guaiacol conversion through the integrated APR-HDO process using methanol or glycerol as the hydrogen source. The characteristic Ni^0 reflections (at 44.5°, 51.8°, and 76.4°) are detected for all the Ni-containing catalysts. However, the 1Ni/AC catalyst also presents NiO's characteristic reflections (at 37.2°, and 62.9°), evidencing Ni oxidation during the reaction. In contrast, no oxidation of the Ni phase could be detected in the XRD patterns of the Ni–Pt/AC catalysts. Therefore, the current results demonstrate a positive effect of Pt in suppressing NiO formation in the bimetallic systems. Such a beneficial effect agrees well with previous studies on PtNi materials reported elsewhere [54,75].

3.5.2. Transmission electron microscopy (TEM)

The TEM micrographs of the spent catalysts, as depicted in Figs. 10 and 11, show the impact of the integrated APR-HDO process and reaction conditions on the morphology of the catalysts. Across all images, an increase in particle size is evident compared to the fresh reduced catalysts (Fig. 2). Intriguingly, the 1Pt/AC catalyst experienced the least morphological change. When comparing the effects of using methanol and glycerol as hydrogen sources on the morphological properties of the active phases, it is clear from Fig. 11 that glycerol has a more substantial impact on nanoparticle morphology. The APR-HDO process with glycerol as the hydrogen source resulted in more pronounced particle aggregation and sintering compared to the process using methanol. However, when examining the spent catalysts from experiments that used methanol as the hydrogen source, it becomes apparent that introducing Pt to the catalyst composition notably mitigated the sintering of the active phase in both Ni–Pt/AC catalysts, when compared to 15Ni/AC catalyst. This indicates the beneficial role of Pt in enhancing the structural stability of Ni–Pt nanoparticles. Overall, these observations demonstrate the significant influence of hydrogen source selection and

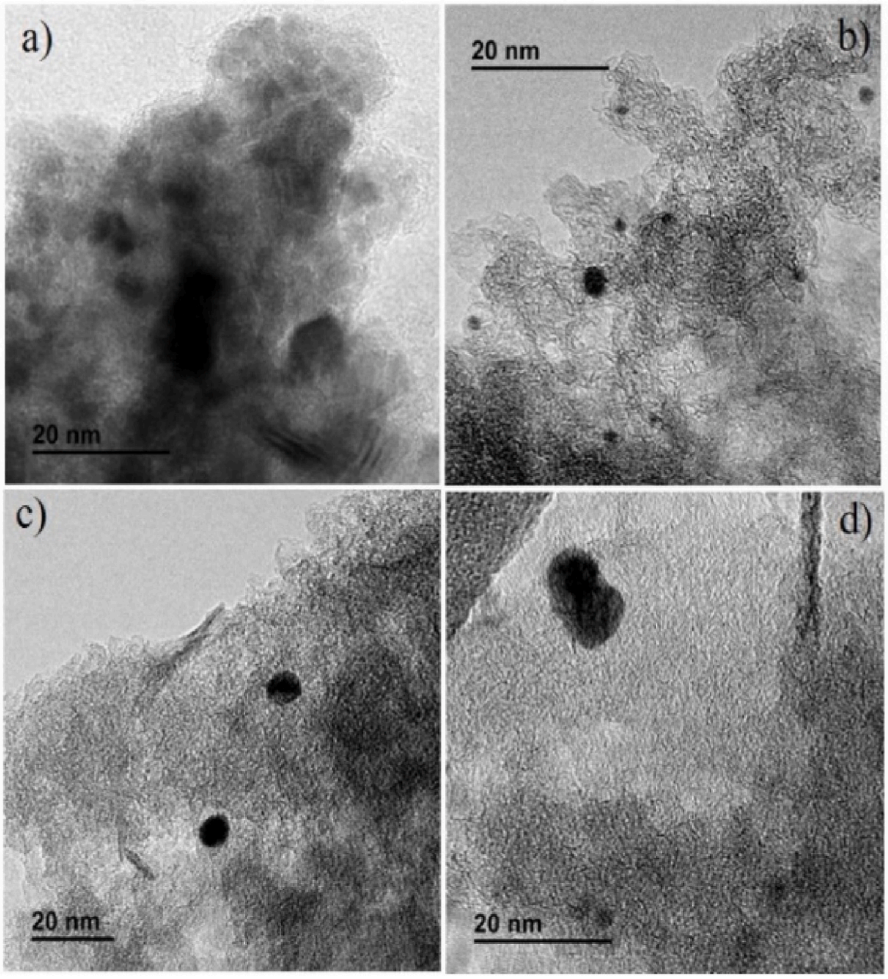

Fig. 11. TEM images of spent catalysts utilised in guaiacol conversion in the integrated APR-HDO process using glycerol as the hydrogen source: a) 15Ni/AC, b) 1Pt/AC, c) 14.5Ni0.5Pt/AC and d) 14Ni1Pt/AC.

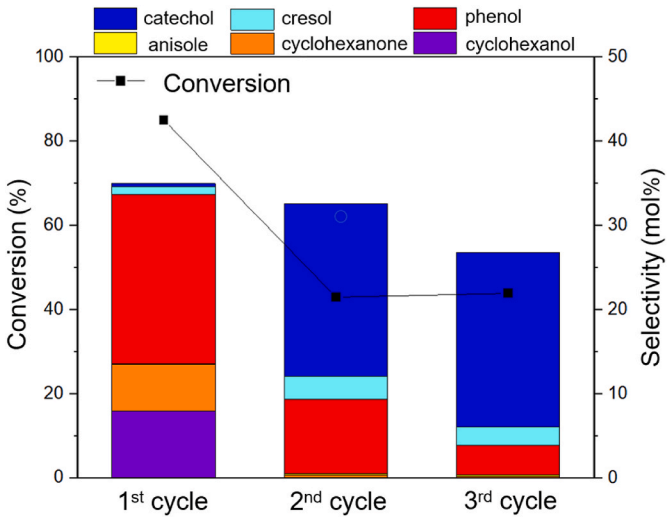

Fig. 12. Recycling test of 14Ni1Pt/AC catalyst using methanol as the hydrogen source. Reaction conditions: guaiacol (0.5 g), methanol (0.5 g) dissolved in water (total mass of 50 g), and catalyst (0.2 g) were processed in a batch reactor (200 mL), operating at 300 °C, 4 h, under an autogenous pressure of 100 bar. The reactor was equipped with an overhead stirrer set at 300 rpm.

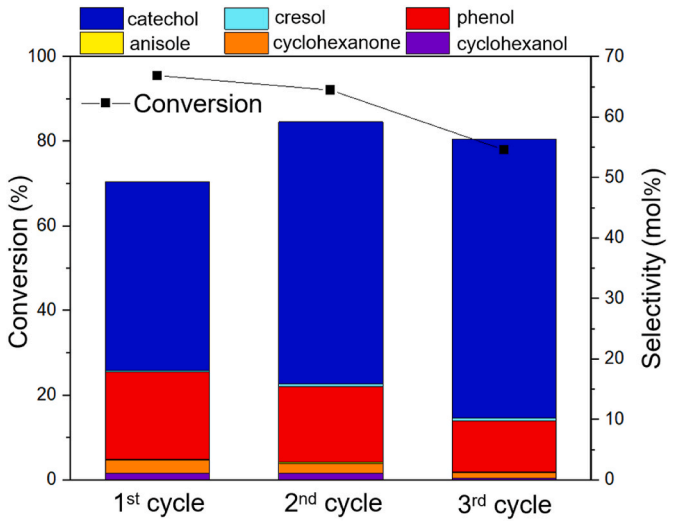

Fig. 13. Recycling test of 1Pt/AC catalyst using glycerol as the hydrogen source. Reaction conditions: guaiacol (0.5 g), glycerol (0.5 g) dissolved in water (total mass of 50 g), and catalyst (0.2 g) were processed in a batch reactor (200 mL), operating at 300 °C, 4 h, under an autogenous pressure of 100 bar. The reactor was equipped with an overhead stirrer set at 300 rpm.

catalyst composition on the stability and performance of the catalysts in the APR-HDO process.

3.6. Catalyst recyclability

Amongst the catalysts evaluated, 14Ni1Pt/AC demonstrated enhanced guaiacol conversion and provided an optimal balance of activity and selectivity when methanol was used as the hydrogen source in the integrated APR-HDO process. In turn, when glycerol was employed as the hydrogen source for the HDO reaction, the 1Pt/AC catalyst exhibited the best balance between activity and selectivity. Building on these findings, we chose to examine the stability of 14Ni1Pt/AC in a catalyst recycling test with methanol as the hydrogen source (Fig. 12) and 1Pt/AC in a similar test using glycerol as the hydrogen source (Fig. 13). Each recycling test consisted of three reaction cycles, with the catalyst undergoing separation, washing, and drying before each cycle.

Fig. 12 summarises the results of the recyclability test of the 14Ni1Pt/AC catalyst, using methanol as the hydrogen source. In the first cycle, the catalyst selectively converts guaiacol into phenol and its hydrogenation products (cyclohexanone and cyclohexanol). In stark contrast, the second and third cycles are characterised by an accumulation of catechol in the product mixture. A decrease in guaiacol conversion from 87 to 43% is observed in the second cycle, stabilising at 43% in the third cycle. This trend aligns well with the metal phase sintering observed after the first cycle, as depicted in Fig. 10. Furthermore, the primary product in the second and third cycles, catechol, is prone to decomposition, decreasing the carbon balance. Consistent with findings from other studies on guaiacol HDO catalysed by nickel phosphide catalysts [81], the coke formed through catechol polymerisation processes can block the catalytic surface for hydrotreatment reactions [82], consequently hindering the saturation of aromatic intermediates.

As shown in Fig. 13, the 1Pt/AC catalyst displays only a minor decrease in guaiacol conversion during the integrated APR-HDO process when glycerol is utilised as the hydrogen source. Interestingly, the selectivity towards phenol and catechol remains largely stable across the evaluation cycles. This result is noteworthy as the decrease in activity and selectivity for HDO processes using glycerol is less pronounced for the 1Pt/AC catalyst, compared to the 14Ni1Pt/AC catalyst when methanol is used as the hydrogen source. This observation, potentially attributable to the strong adsorption of glycerol via a bi/tridentate interaction on metal surfaces, seems to provide some level of protection, as indicated by the less substantial decrease in guaiacol conversion during the integrated APR-HDO process with the 1Pt/AC catalyst using glycerol as the hydrogen source.

4. Conclusions

This study demonstrated the integrated APR-HDO process as a practically viable concept for catalytic upgrading of pyrolysis bio-oil while eliminating the requirement for an external H_2 supply. Regarding catalyst design, the 1Pt/AC catalyst exhibited exceptional performance, achieving a guaiacol conversion exceeding 96% at 300 °C when methanol or glycerol was utilised as the hydrogen source. Conversely, the 15Ni/AC catalyst resulted in a more modest 35% guaiacol conversion under identical conditions. Intriguingly, replacing 0.5–1% of the Ni content with Pt led to bimetallic Ni–Pt/AC catalysts, which displayed an increased guaiacol conversion of up to 70% when methanol was employed as the hydrogen source. However, this enhancement was not replicated when glycerol was used as the hydrogen source. Importantly, Pt played a crucial role in promoting the APR of methanol in generating H_2, thereby meeting H_2 demand required for advancing the HDO extent in the guaiacol conversion towards cyclohexanone and cyclohexanol. As such, the improved guaiacol conversion could be linked to superior APR performance with methanol and, to a lesser extent, glycerol, when Pt was incorporated in the catalyst composition. Nevertheless, glycerol APR was influenced by factors such as particle size, metal distribution, and the Pt^0/Pt^{2+} ratio, which negatively impacted the general performance of the APR-HDO process.

XPS measurements of the reduced catalysts pinpointed a strong interaction between Ni and Pt in the Ni–Pt/AC catalysts. This interaction created NiO_x vacancies; however, it also increased the Ni^0/Ni^{2+} ratio in the reduced Ni–Pt/AC catalyst owing to charge transfer from Pt to Ni. The latter resulted in Pt^{2+} coexisting with Pt^0 species in the reduced Ni–Pt/AC catalysts. These combined features facilitated guaiacol conversion, enhancing the production of cyclohexanol and cyclohexanone, particularly when a 14Ni1Pt/AC catalyst was used with methanol as the hydrogen source.

We also observed that the choice of hydrogen source and the presence of Pt in the catalyst composition significantly influenced catalyst stability within the integrated APR-HDO process. When glycerol was used as the hydrogen source, we noted a higher degree of particle aggregation and sintering than in similar experiments conducted with methanol. Interestingly, the inclusion of Pt in the catalyst composition mitigated this issue, suggesting that Pt positively affected the structural stability of Ni–Pt nanoparticles in the Ni–Pt/AC catalysts.

From a broader perspective, the current results validated the feasibility of integrating APR and HDO processes to eliminate the need for an external high-pressure H_2 supply. This integrated APR-HDO process presents significant advantages in terms of cost and safety, offering considerable promise for the advanced synthetic biofuel sector. This could further stimulate the development of technologies aimed at downsizing catalytic upgrading plants for local pyrolysis oil processing. Utilising methanol as the hydrogen source, the integrated APR-HDO process could act as an initial pretreatment phase, reducing the oxygen content of bio-oils, thus enhancing the stability of bio-oils during storage, and preparing them for subsequent downstream processing in large-scale facilities. Within these larger settings, comprehensive hydrotreatment utilising green H_2 could be conducted in a more cost-effective and safer manner than in decentralised, small-scale facilities.

CRediT authorship contribution statement

Wei Jin: Formal analysis, Investigation, Writing – original draft, preparation. **Jesus Gandara-Loe:** Formal analysis, Investigation, Writing – original draft, preparation. **Laura Pastor-Pérez:** Conceptualizsation, Methodology, Investigation, Writing – original draft, preparation, Visualization, Supervision, Funding acquisition. **Juan J. Villora-Picó:** Formal analysis, All authors have read and agreed to the published version of the manuscript. **Antonio Sepúlveda-Escribano:** Methodology, Investigation, Resources, Writing – review & editing. **Roberto Rinaldi:** Conceptualization, Formal analysis, Resources, Writing – review & editing, Visualization, Supervision, Funding acquisition. **Tomas Ramirez Reina:** Conceptualization, Resources, Funding acquisition, Methodology, Writing – review & editing, Visualization, Supervision, Project administration.

Declaration of competing interest

The authors declare that they have no known competing financial interests or personal relationships that could have appeared to influence the work reported in this paper.

Acknowledgements

Financial support for this work was provided by the Department of Chemical and Process Engineering at the University of Surrey and the EPSRC grant EP/R512904/1 as well as the Royal Society Research Grant RSGR1180353. Authors would also like to acknowledge Spanish Ministry of Science and Innovation through the projects MAT2016-80285-P, RYC2018-024387-I, JC2019-040560-I. RR acknowledges the financial support provided by the ERC Consolidator Grant (LIGNINFIRST, project number 725762). This work was also partially funded by the University

of Seville via the VI PPIT grant scheme for talented researchers and the Junta de Andalucia PAIDI2020 programme through the CLEVER-BIO project P20_00667.

References

[1] S. Oksanen, D. Gielen, S. Kang, R. Leme, T. Masuyama, Advanced Biofuels: what Holds Them Back? International Renewable Energy Agency (IRENA), Abu Dhahi, 2019.

[2] J.L. Field, T.L. Richard, E.A.H. Smithwick, H. Cai, M.S. Laser, D.S. Lebauer, S. P. Long, K. Paustian, Z. Qin, J.J. Sheehan, Robust paths to net greenhouse gas mitigation and negative emissions via advanced biofuels, Proc. Natl. Acad. Sci. USA 117 (2020) 21968–21977.

[3] J. Pretty, Z.P. Bharucha, Sustainable intensification in agricultural systems, Ann. Bot. 114 (2014) 1571–1596.

[4] C.O. Tuck, E. Perez, I.T. Horvath, R.A. Sheldon, M. Poliakoff, Valorization of biomass: deriving more value from waste, Science 337 (2012) 695–699.

[5] E. Furimsky, Catalytic hydrodeoxygenation, Appl. Catal. A 199 (2000) 147–190.

[6] A.V. Bridgwater, Production of high grade fuels and chemicals from catalytic pyrolysis of biomass, Catal. Today 29 (1996) 285–295.

[7] R.R. Soares, D.A. Simonetti, J.A. Dumesic, Glycerol as a source for fuels and chemicals by low-temperature catalytic processing, Angew. Chem. Int. Ed. 45 (2006) 3982–3985.

[8] J.W. Shabaker, G.W. Huber, R.R. Davda, R.D. Cortright, J.A. Dumesic, Aqueous-phase reforming of ethylene glycol over supported platinum catalysts, Catal. Lett. 88 (2003) 1–8.

[9] G.W. Huber, A. Corma, Synergies between bio- and oil refineries for the production of fuels from biomass, Angew. Chem. Int. Ed. 46 (2007) 7184–7201.

[10] J.N. Chheda, G.W. Huber, J.A. Dumesic, Liquid-phase catalytic processing of biomass-derived oxygenated hydrocarbons to fuels and chemicals, Angew. Chem., Int. Ed. Engl. 46 (2010) 7164–7183.

[11] M.D. Boot, M. Tian, E. Hensen, S.M. Sarathy, Impact of fuel molecular structure on auto-ignition behavior-Design rules for future high performance gasolines, Prog. Energy Combust. Sci. 60 (2017) 1–25.

[12] B. Sugiarto, M.F. Dwinanda, D. Auliady, R.N. Andito, Mokhtar, C.R. M. Simanjuntak, Investigation of cyclohexanol as an oxygenated additive for gasoline-Bioethanol mixtures and its effect on the combustion and emission characteristics of spark ignition engines, Int. J. Technol. 12 (2021) 1071–1080.

[13] Y. Devarajan, A. Mahalingam, D.B. Munuswamy, B. Nagappan, Emission and combustion profile study of unmodified research engine propelled with neat biofuels, Environ. Sci. Pollut. Res. 25 (2018) 19643–19656.

[14] M. Gulum, A. Bilgin, Two-dimensionl surface models to predict the density of biodiesel-diesel-alcohol ternary blends, Energy Sources, Part A. Recovery, Utilization, and Environmrntal Effects 43 (2021) 517–587.

[15] A. Bilgin, M. Gulum, Effects of various transesterification parameters on some fuel properties of hazelnut oil methyl ester, International Scientific Conference Environmental and Climate Technologies, Conect 147 (2018) 54–62.

[16] B. Suresh, R. Gubler, Y. Yamaguchi, X. He, Hydrogen Market Research: Hydrogen Market Outlook, Supply & Demand, Forecast and Analysis. Chemical Economics Handbook, I Markit, 2013.

[17] F. Schueth, Hydrogen: economics and its role in biorefining, in: Catalytic Hydrogenation for Biomass Valorization, R. Rinaldi, The Royal Society of Chemistry, 2014, pp. 1–21.

[18] G.W. Huber, P. O'Connor, A. Corma, Processing biomass in conventional oil refineries: production of high quality diesel by hydrotreating vegetable oils in heavy vacuum oil mixtures, Appl. Catal. A 329 (2007) 120–129.

[19] Z. Cao, M. Dierks, M.T. Clough, I. Castro, R. Rinaldi, A convergent approach for a deep converting lignin-First biorefinery rendering high-energy-density drop-in fuels, Joule 2 (2018) 1118–1133.

[20] W. Jin, L. Pastor-Pérez, D. Shen, A. Sepúlveda-Escribano, S. Gu, T. Ramirez Reina, Catalytic upgrading of biomass model compounds: novel approaches and lessons learnt from traditional hydrodeoxygenation–a review, ChemCatChem 11 (2019) 924–960.

[21] J.S. Moon, Y.K. Lee, Support effects of Ni2P catalysts on the hydrodeoxygenation of guaiacol: in situ XAFS studies, Top. Catal. 58 (2015) 211–218.

[22] X. Liu, W. An, Y. Wang, C.H. Turner, D. Resasco, Hydrodeoxygenation of guaiacol over bimetallic Fe-alloyed (Ni, Pt) surfaces: reaction mechanism, transition-state scaling relations and descriptor for predicting C–O bond scission reactivity, Catal. Sci. Technol. 8 (2018) 2146–2158.

[23] Y. Hong, H. Zhang, J. Sun, K.M. Ayman, A.J.R. Hensley, M. Gu, M.H. Engelhard, J. S. Mcewen, Y. Wang, Synergistic catalysis between Pd and Fe in gas phase hydrodeoxygenation of m-cresol, ACS Catal. 4 (2014) 3335–3345.

[24] C. Li, X. Zhao, A. Wang, G.W. Huber, Z. Tao, Catalytic transformation of lignin for the production of chemicals and fuels, Chem. Rev. 115 (2015) 11559–11624.

[25] W. Yu, M.D. Porosoff, J.G. Chen, Review of Pt-based bimetallic catalysis: from model surfaces to supported catalysts, Chem. Rev. 112 (2012) 5780–5817.

[26] H. Chen, X. Zhang, J. Zhang, Q. Wang, Tuning the decarboxylation selectivity for deoxygenation of vegetable oil over Pt–Ni bimetal catalysts via surface engineering, Catal. Sci. Technol. 8 (2018) 1126–1133.

[27] H. Chen, X. Zhang, Q. Wang, Hydroconversion of C18 fatty acids using PtNi/Al2O3: insight in the role of hydroxyl groups in Al_2O_3, Catal. Commun. 97 (2017) 14–17.

[28] H. Chen, S. Yao, W. Lin, Z. Zhang, X. Hu, X. Liu, B. Yan, K. Chen, Y. Qin, Y. Zhu, Highly efficient conversion of oleic acid to heptadecane without external hydrogen source over atomic layer deposited bimetallic Ni-Pt catalysts, Chem. Eng. J. 390 (2020), 124603.

[29] S.K. Singh, J.D. Ekhe, Towards effective lignin conversion: HZSM-5 catalysed one-pot solvolytic depolymerisation/hydrodeoxygenation of lignin into value added compounds, RSC Adv. 4 (2014) 27971–27978.

[30] R. Rinaldi, R. Jastrzebski, M.T. Clough, J. Ralph, M. Kennema, P. Bruijnincx, B. M. Weckhuysen, Paving the way for lignin valorisation: recent advances in bioengineering, biorefining and catalysis, Angew. Chem. Int. Ed. 55 (2016) 8164–8215.

[31] M.M. Abu-Omar, K. Barta, G.T. Beckham, J. Luterbacher, Guidelines for performing lignin-first biorefining, F. Wang, Energy Environ. Sci. 14 (2021) 262–292.

[32] W. Song, Y. Liu, E. Baráth, C. Zhao, J.A. Lercher, Synergistic effects of Ni and acid sites for hydrogenation and C–O bond cleavage of substituted phenols, Green Chem. 17 (2015) 1204–1218.

[33] X. Li, G. Chen, C. Liu, W. Ma, B. Yan, J. Zhang, Hydrodeoxygenation of lignin-derived bio-oil using molecular sieves supported metal catalysts: a critical review, Renew. Sustain. Energy Rev. 71 (2017) 296–308.

[34] Y. Huang, Y. Hu, F. Ye, Y. Fang, Lignin Pyrolysis and in situ hydrodeoxygenation over MoO_3: interaction between MoO_3 and lignin, Energy Fuels 31 (2017) 8356–8362.

[35] P. de Wild, W. Huijgen, A. Kloekhorst, R. Chowdari, H. Heeres, Biobased alkylphenols from lignins via a two-step pyrolysis–Hydrodeoxygenation approach, Bioresour. Technol. 229 (2017) 160–168.

[36] X. Zhang, W. Tang, Q. Zhang, T. Wang, L. Ma, Hydrodeoxygenation of lignin-derived phenoic compounds to hydrocarbon fuel over supported Ni-based catalysts, Appl. Energy 227 (2018) 73–79.

[37] C. Ju, M. Li, Y. Fang, T. Tan, Efficient hydro-deoxygenation of lignin derived phenolic compounds over bifunctional catalysts with optimised acid/metal interactions, Green Chem. 20 (2018) 4492–4499.

[38] M.M. Ambursa, P. Sudarsanam, L.H. Voon, S.B.A. Hamid, S.K. Bhargava, Bimetallic Cu-Ni catalysts supported on MCM-41 and Ti-MCM-41 porous materials for hydrodeoxygenation of lignin model compound into transportation fuels, Fuel Process. Technol. 162 (2017) 87–97.

[39] R.D. Cortright, R. Davda, J.A. Dumesic, Hydrogen from catalytic reforming of biomass-derived hydrocarbons in liquid water, Mater. Sustain. Energy 33 (2010) 289–292.

[40] Y. Guo, X. Liu, M.U. Xu, W. Azmat, J. Ren, Y. Wang, G. Lu, Hydrogen production by aqueous-phase reforming of glycerol over Ni-B catalyst, Fuel Energy Abstr. 37 (2012) 227–234.

[41] M. Wang, M.J. Liu, F. Wang, Photo splitting of bio-polyols and sugars to methanol and syngas, Nat. Commun. 11 (2020) 1083.

[42] M.H. Haider, N.F. Dummer, D.W. Knight, R.L. Jenkins, M. Howard, J. Moulijn, S. H. Taylor, G.J. Hutchings, Efficient green methanol synthesis from glycerol, Nat. Chem. 7 (2015) 1028–1032.

[43] V.L. Yfanti, E.S. Vasiliadou, A. Lemonidou, Tandem Catalytic Reactions of Methanol Aqueous Reforming - Glycerol Hydrodeoxygenation Targeted to Selective 1,2-propanediol Formation, 3rd International Symposium on Green Chemistry, 2015.

[44] V.L. Yfanti, E.S. Vasiliadou, A. Lemonidou, Catalytic Hydrodeoxygenation of Glycerol Aided by In-Situ H_2 Generation from Methanol, 24th North American Society Meeting, 2015.

[45] J.F. Feng, Chung-yun, Hse, Z.Z. Yang, K. Wang, J.C. Jiang, Liquid phase in situ hydrodeoxygenation of biomass-derived phenolic compounds to hydrocarbons over bifunctional catalysts, Appl. Catal. A 542 (2017) 163–173.

[46] G. Wen, Y. Xu, H. Ma, Z. Xu, Z. Tian, Production of hydrogen by aqueous-phase reforming of glycerol, Int. J. Hydrogen Energy 33 (2008) 6657–6666.

[47] E.S. Vasiliadou, V.-L. Yfanti, A. Lemonidou, One-pot tandem processing of glycerol stream to 1, 2-propanediol with methanol reforming as hydrogen donor reaction, Appl. Catal., B 163 (2015) 258–266.

[48] W. Jin, L. Pastor-Pérez, J.J. Villora-Pico, M.M. Pastor-Blas, A. Sepúlveda-Escribano, S. Gu, N.D. Charisiou, K. Papageridis, M.A. Goula, T.R. Reina, Catalytic conversion of palm oil to bio-hydrogenated diesel over novel N-doped activated carbon supported Pt nanoparticles, Energies 13 (2020) 132.

[49] J. Wei, L. Pérez, J. Villora-Picó, A. Sepúlveda-Escribano, T.R. Reina, Investigating new routes for biomass upgrading: "H_2-free" HDO using Ni-based catalysts, ACS Sustain. Chem. Eng. 7 (2019) 16041–16049.

[50] L. Pérez, J. Wei, J. Villora-Picó, M.M. Pastor-Blas, T.R. Reina, "H_2-free" demethoxylation of guaiacol in subcritical water using Pt supported on N-doped carbon catalysts: a cost-effective strategy for biomass upgrading, J. Energy Chem. 58 (2021) 377–385.

[51] R. Olcese, M. Bettahar, D. Petitjean, B. Malaman, F. Giovanella, A. Dufour, Gas-phase hydrodeoxygenation of guaiacol over Fe/SiO_2 catalyst, Appl. Catal., B 115 (2012) 63–73.

[52] J. Santos, M. Alda-Onggar, V. Fedorov, M. Peurla, K. Eränen, P. Mäki-Arvela, M.Á. Centeno, D.Y. Murzin, Hydrodeoxygenation of vanillin over carbon supported metal catalysts, Appl. Catal. A 561 (2018) 137–149.

[53] X. Kong, Y. Zhu, H. Zheng, X. Li, Y. Zhu, Y.-W. Li, Ni nanoparticles inlaid nickel phyllosilicate as a metal–acid bifunctional catalyst for low-temperature hydrogenolysis reactions, ACS Catal. 5 (2015) 5914–5920.

[54] E. Le Saché, J. Santos, T. Smith, M. Centeno, H. Arellano-Garcia, J.A. Odriozola, T. Reina, Multicomponent Ni-CeO 2 nanocatalysts for syngas production from CO_2/CH_4 mixtures, J. CO_2 Util. 25 (2018) 68–78.

[55] L. García-Cerda, K. Bernal-Ramos, S.M. Montemayor, M. Quevedo-López, R. Betancourt-Galindo, D. Bueno-Báques, Preparation of hcp and fcc Ni and Ni/NiO

nanoparticles using a citric acid assisted pechini-type method, J. Nanomater. 2011 (2011) 72.
[56] H.A. Huy, T. Van Man, H.T. Tai, H.T.T. Van, Preparation and characterisation of high-dispersed pt/c nano-electrocatalysts for fuel cell applications, Vietnam J. Sci. Technol. 54 (2016) 472.
[57] J. Rynkowski, D. Rajski, I. Szyszka, J.R. Grzechowiak, Effect of platinum on the hydrogenation activity of nickel catalysts, Catal. Today 90 (2004) 159–166.
[58] N.-Y. Chen, M.-C. Liu, S.-C. Yang, J.-R. Chang, EXAFS peaks and TPR characterising bimetallic interactions: effects of impregnation methods on the structure of Pt-Ru/C catalysts, J Spectrosc 2014 (2014), 347078.
[59] Q. Ma, W. Ding, M. Wu, T. Zhao, N. Tsubaki, Effect of catalytic site position: nickel nanocatalyst selectively loaded inside or outside carbon nanotubes for methane dry reforming, Fuel 108 (2013) 430–438.
[60] Katarína Fabiovicová, Oliver Malter, Martin Lucas, Peter Claus, Hydrogenolysis of cellulose to valuable chemicals over activated carbon supported mono- and bimetallic nickel/tungsten catalysts, Green Chem. 16 (2014) 3580–3588.
[61] P. Burattin, M. Che, C. Louis, Ni/SiO_2 materials prepared by Deposition−Precipitation: influence of the reduction conditions and mechanism of formation of metal particles, J. Phys. Chem. B 105 (2000) 10482–10489.
[62] M. El Doukkali, A. Iriondo, P. Arias, J. Requies, I. Gandarías, L. Jalowiecki-Duhamel, F. Dumeignil, A comparison of sol–gel and impregnated Pt or/and Ni based γ-alumina catalysts for bioglycerol aqueous phase reforming, Appl. Catal., B 125 (2012) 516–529.
[63] V.M. Shinde, G. Madras, Nanostructured Pd modified Ni/CeO_2 catalyst for water gas shift and catalytic hydrogen combustion reaction, Appl. Catal., B 132 (2013) 28–38.
[64] I. Czekaj, F. Loviat, F. Raimondi, J. Wambach, S. Biollaz, A. Wokaun, Characterisation of surface processes at the Ni-based catalyst during the methanation of biomass-derived synthesis gas: X-ray photoelectron spectroscopy (XPS), Appl. Catal. A 329 (2007) 68–78.
[65] Z. Boukha, C. González, M.G. Calvo, B.D. Rivas, R.L. Fonseca, MgO/$NiAl_2O_4$ as a new formulation of reforming catalysts: tuning the surface properties for the enhanced partial oxidation of methane, Appl. Catal., B 199 (2016) 372–383.
[66] L. Huang, Y. Lv, S. Wu, P. Liu, W. Xiong, F. Hao, H. Luo, Activated carbon supported bimetallic catalysts with combined catalytic effects for aromatic nitro compounds hydrogenation under mild conditions, Appl. Catal. A 577 (2019) 76–85.
[67] M.M. Telkar, J.M. Nadgeri, C.V. Rode, R.V. Chaudhari, Role of a co-metal in bimetallic Ni–Pt catalyst for hydrogenation of m-dinitrobenzene to m-phenylenediamine, Appl. Catal. A 295 (2005) 23–30.
[68] L. Lin, Z. Wu, G. Rui, S. Yao, M. Ding, Low-Temperature hydrogen production from water and methanol using Pt/α-MoC catalysts, Nature 544 (2017) 80–83.
[69] X. Wang, R. Rinaldi, Exploiting H-transfer reactions with RANEY® Ni for upgrade of phenolic and aromatic biorefinery feeds under unusual, low-severity conditions, Energy Environ. Sci. 5 (2012) 8244–8260.
[70] X. Wang, R. Rinaldi, Solvent effects on the hydrogenolysis of diphenyl ether with Raney nickel and their implications for the conversion of lignin, ChemSusChem 5 (2012) 1455–1466.
[71] J. Callison, N. Subramanian, S. Rogers, A. Chutia, D. Gianolio, C.R.A. Catlow, P. P. Wells, N. Dimitratos, Directed aqueous-phase reforming of glycerol through tailored platinum nanoparticles, Appl. Catal., B 238 (2018) 618–628.
[72] A. Vikla, I. Simakova, Y. Demidova, E. Keim, L. Calvo, M. Gilarranz, S. He, K. Seshan, Tuning Pt characteristics on Pt/C catalyst for aqueous-phase reforming of biomass-derived oxygenates to bio-H_2, Appl. Catal. A 610 (2021), 117963.
[73] A. Bjelić, M. Grilc, M. Huš, B. Likozar, Hydrogenation and hydrodeoxygenation of aromatic lignin monomers over Cu/C, Ni/C, Pd/C, Pt/C, Rh/C and Ru/C catalysts: mechanisms, reaction micro-kinetic modelling and quantitative structure-activity relationships, Chem. Eng. J. 359 (2019) 305–320.
[74] A. Wawrzetz, B. Peng, A. Hrabar, A. Jentys, A.A. Lemonidou, J.A. Lercher, Towards understanding the bifunctional hydrodeoxygenation and aqueous phase reforming of glycerol, J. Catal. 269 (2010) 411–420.
[75] M. Kennema, I.D. Castro, F. Meemken, R. Rinaldi, On the liquid-phase H-transfer from 2-propanol to phenol on raney Ni: surface processes and inhibition, ACS Catal. 7 (2017) 2437–2445.
[76] L. Faba, E. Díaz, S. Ordóez, Role of the support on the performance and stability of Pt-based catalysts for furfural–acetone adduct hydrodeoxygenation, Catal. Sci. Technol. 5 (2015) 1473.
[77] P.T. Witte, P.H. Berben, S. Boland, E.H. Boymans, D. Vogt, J.W. Geus, J. G. Donkervoort, Basf NanoSelect Technology, Innovative supported Pd- and Pt-based catalysts for selective hydrogenation reactions, Top. Catal. 55 (2012) 505–511.
[78] Z. Liu, I.A. Hamad, Y. Li, Y. Chen, S. Wang, R.E. Jentoft, F.C. Jentoft, Poisoning and competitive adsorption effects during phenol hydrogenation on platinum in water-alcohol mixtures, Appl. Catal. Gen. 585 (2019), 117199.
[79] X. He, Y. Xu, X. Yao, C. Zhang, Y. Pu, X. Wang, W. Mao, Y. Du, W. Zhong, Large exchange bias and enhanced coercivity in strongly-coupled Ni/NiO binary nanoparticles, RSC Adv. 9 (2019) 30195–30206.
[80] I. Graça, R.T. Woodward, M. Kennema, R. Rinaldi, Formation and fate of carboxylic acids in the lignin-first biorefining of lignocellulose via H-transfer catalyzed by raney Ni, ACS Sustain. Chem. Eng. 6 (2018) 13408–13419.
[81] M. Dierks, Z. Cao, R. Rinaldi, Design of task-specific metal phosphides for the sustainable manufacture of advanced biofuels, Adv. Inorg. Chem. 77 (2021) 219–239.
[82] G.Y. Chen, W.Q. Li, H. Chen, B.B. Yan, Progress in the aqueous-phase reforming of different biomass-derived alcohols for hydrogen production, J. Zhejiang Univ. - Sci. A 16 (2015) 491–506.
[83] M. Kennema, I.D. Castro, F. Meemken, R. Rinaldi, Liquid-phase H-transfer from 2-propanol to phenol on raney Ni: surface processes and inhibition, ACS Catal. 7 (2017) 2437–2445.